

A Hybrid Artificial Intelligence and Two Dimensional Depth Averaged Numerical Model for Solving Shallow Water and Exner Equations Simultaneously

S. Mehrab Amiri, Nasser Talebbeydokhti

Abstract—Modeling sediment transport processes by means of numerical approach often poses severe challenges. In this way, a number of techniques have been suggested to solve flow and sediment equations in decoupled, semi-coupled or fully coupled forms. Furthermore, in order to capture flow discontinuities, a number of techniques, like artificial viscosity and shock fitting, have been proposed for solving these equations which are mostly required careful calibration processes. In this research, a numerical scheme for solving shallow water and Exner equations in fully coupled form is presented. First-Order Centered scheme is applied for producing required numerical fluxes and the reconstruction process is carried out toward using Monotonic Upstream Scheme for Conservation Laws to achieve a high order scheme. In order to satisfy C-property of the scheme in presence of bed topography, Surface Gradient Method is proposed. Combining the presented scheme with fourth order Runge-Kutta algorithm for time integration yields a competent numerical scheme. In addition, to handle non-prismatic channels problems, Cartesian Cut Cell Method is employed. A trained Multi-Layer Perceptron Artificial Neural Network which is of Feed Forward Back Propagation (FFBP) type estimates sediment flow discharge in the model rather than usual empirical formulas. Hydrodynamic part of the model is tested for showing its capability in simulation of flow discontinuities, transcritical flows, wetting/drying conditions and non-prismatic channel flows. In this end, dam-break flow onto a locally non-prismatic converging-diverging channel with initially dry bed conditions is modeled. The morphodynamic part of the model is verified simulating dam break on a dry movable bed and bed level variations in an alluvial junction. The results show that the model is capable in capturing the flow discontinuities, solving wetting/drying problems even in non-prismatic channels and presenting proper results for movable bed situations. It can also be deduced that applying Artificial Neural Network, instead of common empirical formulas for estimating sediment flow discharge, leads to more accurate results.

Keywords—Artificial neural network, morphodynamic model, sediment continuity equation, shallow water equations.

I. INTRODUCTION

MODELING of bedload sediment transport processes in alluvial channels is one of the major concerns in open channel hydraulics community. The two main approaches for this purpose include physical and numerical models. Despite of their advantages, the physical models usually consume

much time and cost, then applying numerical approaches is increasing rapidly, especially in presence of powerful computers.

Most of the numerical models solve a combination of hydrodynamics and sediment continuity equations [1]-[6]. In two dimensional forms, the hydrodynamic part of the model is usually handled by the classical non-linear shallow-water equations (NLSW), while Exner equation governs the sediment continuity part.

A large amount of work has been conducted in the last decades to develop numerical methods for solving NLSW. A challenging problem that should be resolved is how the flow discontinuity is captured. To this end, a number of techniques like artificial viscosity (particularly for finite difference methods) and shock fitting have been proposed. These techniques usually require ad-hoc terms which need to be carefully calibrated.

Estimation of sediment transport discharge, as required by Exner equation, has been formulated through empirical relationships, each defined for specific experimental situations. Evidently, employing an empirical formula out of its domain of governance may lead to undesirable outcomes. However, during sediment transport processes, the problem situations may be altered. Consequently, an alternative technique with fewer amounts of limitations may present better results.

In the context of numerical models, the combination of shallow water and Exner equations can be solved either in fully coupled, semi-coupled or uncoupled form. Previous studies show the efficiency of fully coupled approach in which NLSW and Exner equations are solved simultaneously [7].

In this research, a numerical scheme for solving NLSW and Exner equations in fully coupled form is presented. The model employs Monotonic Upstream Scheme for Conservation Laws (MUSCL) for estimating flow variables in the cell interfaces and First-Order Centered (FORCE) scheme for producing required numerical fluxes. Surface Gradient Method (SGM) in combination with fourth order Runge-Kutta algorithm for time integration can guarantee to have a well-balance model. Furthermore, Cartesian Cut Cell Method (CCCM) makes it possible to apply this model for non-prismatic channels. A trained Multi-Layer Perceptron (MLP) Artificial Neural Network (ANN) which is of FFBP type is applied for estimating sediment flow rate in the model.

The hydrodynamic part of the model is verified through several examples such as transcritical flow over a bump with

S. Mehrab Amiri is Assistant Professor of Department of Civil and Environmental Engineering, Shiraz University, Shiraz, Iran (corresponding author, phone: +989173080061, e-mail: mamiri@shirazu.ac.ir).

Nasser Talebbeydokhti is Professor of Department of Civil and Environmental Engineering, Shiraz University, Shiraz, Iran (phone: +989171179407, e-mail: taleb@shirazu.ac.ir).

and without shock, subcritical flow over a bump and dam-break on a dry bed channel with varying width. Then, the fully coupled model is employed for simulation of dune movement, dam break on a dry movable bed and bed level variations in an alluvial junction.

II. GOVERNING EQUATIONS

Hydrodynamic part of the model is based on NLSW equations. The conservative form of NLSW equations is written as:

$$\frac{\partial h}{\partial t} + \frac{\partial(Uh)}{\partial x} + \frac{\partial(Vh)}{\partial y} = 0 \quad (1)$$

$$\frac{\partial(Uh)}{\partial t} + \frac{\partial}{\partial x} \left(U^2 h + \frac{1}{2} g h^2 \right) + \frac{\partial(UVh)}{\partial y} - g h \frac{\partial z_b}{\partial x} - \frac{\tau_{bx}}{\rho} + \frac{1}{\rho} \frac{\partial}{\partial x} (h \tau_{xx}) + \frac{1}{\rho} \frac{\partial}{\partial y} (h \tau_{xy}) \quad (2)$$

$$\frac{\partial(Vh)}{\partial t} + \frac{\partial}{\partial y} \left(V^2 h + \frac{1}{2} g h^2 \right) + \frac{\partial(UVh)}{\partial x} - g h \frac{\partial z_b}{\partial y} - \frac{\tau_{by}}{\rho} + \frac{1}{\rho} \frac{\partial}{\partial y} (h \tau_{yy}) + \frac{1}{\rho} \frac{\partial}{\partial x} (h \tau_{yx}) \quad (3)$$

In these equations, t denotes time, x is the longitudinal distance, y is the span-wise distance, ρ is the water density, h is the water depth, z_b is the bottom elevation, U is the depth-averaged velocity along x -direction, V is the depth-averaged velocity along y -direction, and g is the gravitational acceleration. τ_{bx} , τ_{by} are the friction stresses which are included using the Manning's resistance law:

$$\frac{\tau_{bx}}{\rho} = \frac{g n_{Manning}^2 U \sqrt{U^2 + V^2}}{h^{1/3}}, \quad \frac{\tau_{by}}{\rho} = \frac{g n_{Manning}^2 V \sqrt{U^2 + V^2}}{h^{1/3}} \quad (4)$$

in which, $n_{Manning}$ denotes the Manning's friction coefficient. τ_{xx} , τ_{xy} , τ_{yy} and τ_{yx} are the Reynolds Shear Stresses which are defined as follows:

$$\tau_{xx} = \frac{2}{h} \rho \nu_{ff} \frac{\partial(hU)}{\partial x} \quad (5)$$

$$\tau_{xy} = \tau_{yx} = \frac{1}{h} \rho \nu_{ff} \left[\frac{\partial(hU)}{\partial y} + \frac{\partial(hV)}{\partial x} \right] \quad (6)$$

where ν_{ff} is the effective turbulence kinematic viscosity. Smagorinsky presented the following relationship for ν_{ff} [8]:

$$\nu_{ff} = \alpha * \Delta x * \Delta y \sqrt{\left(\frac{\partial U}{\partial x}\right)^2 + \left(\frac{\partial V}{\partial y}\right)^2 + 0.5 \left(\frac{\partial U}{\partial y} + \frac{\partial V}{\partial x}\right)^2} \quad (8)$$

Δx is the cell size in x direction, Δy is the cell size in y direction and α is a dimensionless coefficient which is suggested about 0.1 for shallow water conditions. (1) to (3) can be written either in the following form:

$$\frac{\partial \mathbf{U}}{\partial t} + \frac{\partial \mathbf{F}(\mathbf{U})}{\partial x} + \frac{\partial \mathbf{G}(\mathbf{U})}{\partial y} = \mathbf{S}(\mathbf{U}) \quad (9)$$

where the vector of conserved flow variables, \mathbf{U} , the flux vectors, $\mathbf{F}(\mathbf{U})$ and $\mathbf{G}(\mathbf{U})$, and the source term vector, $\mathbf{S}(\mathbf{U})$, are defined, respectively, as:

$$\mathbf{U} = \begin{bmatrix} h \\ hU \\ hV \end{bmatrix}, \quad \mathbf{F}(\mathbf{U}) = \begin{bmatrix} hU \\ hU^2 + \frac{1}{2}gh^2 \\ hUV \end{bmatrix}, \quad \mathbf{G}(\mathbf{U}) = \begin{bmatrix} hV \\ hUV \\ hV^2 + \frac{1}{2}gh^2 \end{bmatrix}, \quad (10)$$

$$\mathbf{S}(\mathbf{U}) = \begin{bmatrix} 0 \\ -gh \frac{\partial z_b}{\partial x} - \frac{\tau_{bx}}{\rho} + \frac{1}{\rho} \frac{\partial}{\partial x} (h \tau_{xx}) + \frac{1}{\rho} \frac{\partial}{\partial y} (h \tau_{xy}) \\ -gh \frac{\partial z_b}{\partial y} - \frac{\tau_{by}}{\rho} + \frac{1}{\rho} \frac{\partial}{\partial y} (h \tau_{yy}) + \frac{1}{\rho} \frac{\partial}{\partial x} (h \tau_{yx}) \end{bmatrix}$$

The sediment transport processes part of the model is presented through applying Exner equation:

$$\frac{\partial z_b}{\partial t} + \frac{1}{1-m} \frac{\partial q_{sx}}{\partial x} + \frac{1}{1-m} \frac{\partial q_{sy}}{\partial y} = 0 \quad (11)$$

where q_{sx} and q_{sy} are the total bed load sediment transport discharge in x and y directions, respectively, and m is the bed material porosity.

For fully coupled morphodynamic model, flow variables, the flux vectors and the source term vector, are defined as:

$$\mathbf{U} = \begin{bmatrix} h \\ hU \\ hV \\ z_b \end{bmatrix}, \quad \mathbf{F}(\mathbf{U}) = \begin{bmatrix} hU \\ hU^2 + \frac{1}{2}gh^2 \\ hUV \\ \frac{1}{m-1} q_{sx} \end{bmatrix}, \quad \mathbf{G}(\mathbf{U}) = \begin{bmatrix} hV \\ hUV \\ hV^2 + \frac{1}{2}gh^2 \\ \frac{1}{m-1} q_{sy} \end{bmatrix}, \quad (12)$$

$$\mathbf{S}(\mathbf{U}) = \begin{bmatrix} 0 \\ -gh \frac{\partial z_b}{\partial x} - \frac{\tau_{bx}}{\rho} + \frac{1}{\rho} \frac{\partial}{\partial x} (h \tau_{xx}) + \frac{1}{\rho} \frac{\partial}{\partial y} (h \tau_{xy}) \\ -gh \frac{\partial z_b}{\partial y} - \frac{\tau_{by}}{\rho} + \frac{1}{\rho} \frac{\partial}{\partial y} (h \tau_{yy}) + \frac{1}{\rho} \frac{\partial}{\partial x} (h \tau_{yx}) \\ 0 \end{bmatrix}$$

III. MODEL IMPLEMENTATION

Due to some special aspects of the governing equations, several considerations should be taken into account to achieve numerical solutions. In the first step, the hydrodynamic part is regarded to obtain efficient numerical model for flow, and then, the results are generalized for fully coupled form of the

equations.

Several characteristics of conservative form of the NLSW equations such as nonlinearity and hyperbolicity, often give rise to discontinuous solutions such as bores and hydraulic jumps. The integral representation of governing PDEs is preferred under such circumstances, because smoothness of solution is not a necessary requirement by this formulation.

The system of (9) can be rewritten as:

$$\frac{\partial \mathbf{U}}{\partial t} + \nabla \cdot \mathbf{E} = \mathbf{S}(\mathbf{U})$$

$$\mathbf{E} = F\vec{i} + G\vec{j} \quad (13)$$

Finite volume method in the cell-centered form is formulated for the equation, by integrating over a typical finite area of A_i . Then, the integral form of the equation is:

$$\iint_{A_i} \frac{\partial \mathbf{U}}{\partial t} dA + \iint_{A_i} \nabla \cdot \mathbf{E} dA = \iint_{A_i} \mathbf{S} dA \quad (14)$$

Employing divergence theorem for the second integral term of (14), it can be replaced by:

$$\iint_{A_i} \frac{\partial \mathbf{U}}{\partial t} dA + \oint_{\Gamma_i} \mathbf{E} \cdot \mathbf{n} d\Gamma = \iint_{A_i} \mathbf{S} dA \quad (15)$$

Γ_i is boundary of the i th finite area A_i , and \mathbf{n} is the outward unit vector normal to the boundary. Equation (15) can be approximated through using midpoint quadrature rule:

$$\frac{dU_i}{dt} = -\frac{1}{A_i} \sum_{j=1}^m E^* \cdot \vec{n}_{ij} \Delta \Gamma_{ij} + S_i \quad (16)$$

in which i denotes i th computational cell, j indicates j th edge of the cell, m is the number of edges, U_i and S_i are the averaged quantities at center of the cell, $\Delta \Gamma_{ij}$ is the length of the j th edge of the i th cell and E^* is numerical flux through the edge which will be calculated using FORCE scheme. Through a few mathematical manipulations, for a rectangular computational cell with length and width of Δx and Δy , (16) can be discretized in the difference form as:

$$\frac{U_{i,j}^{n+1} - U_{i,j}^n}{\Delta t} = -\frac{F_{i+(1/2),j} - F_{i-(1/2),j}}{\Delta x} - \frac{G_{i,j+(1/2)} - G_{i,j-(1/2)}}{\Delta y} + S_{i,j} \quad (17)$$

where Δt is time step, subscripts i, j refers to i, j -th cell center and superscript n and $n+1$ refer to current (known) and next (unknown) time levels, respectively. $F_{i+(1/2),j}$, $F_{i-(1/2),j}$, $G_{i,j+(1/2)}$ and $G_{i,j-(1/2)}$ are numerical fluxes at cell interfaces $i+(1/2), j$, $i-(1/2), j$, $i, j+(1/2)$ and

$i, j-(1/2)$, respectively.

Following integration form of the flow governing equations, an extrapolating method is required to prepare proper variables to compute the interface fluxes. For this purpose, the FORCE Scheme can be used. This scheme was first introduced by [9] and found to be robust in applications and simple to implement. The FORCE flux actually holds by simple averaging of the Lax–Friedrichs (LF) and two-step Lax–Wendroff (LW) fluxes. As shown by [9], the FORCE scheme is an optimal scheme through the family of three-point schemes that can be written as the convex average of the LF and LW fluxes [10].

$$F_{i+(1/2),j}^{\text{FORCE}} = \frac{1}{2}(F_{i+(1/2),j}^{\text{LF}} + F_{i+(1/2),j}^{\text{LW}})$$

$$G_{i,j+(1/2)}^{\text{FORCE}} = \frac{1}{2}(G_{i,j+(1/2)}^{\text{LF}} + G_{i,j+(1/2)}^{\text{LW}}) \quad (18)$$

where $F_{i+(1/2),j}^{\text{LF}}$ and $G_{i,j+(1/2)}^{\text{LF}}$ are the Lax–Friedrichs fluxes and $F_{i+(1/2),j}^{\text{LW}}$ and $G_{i,j+(1/2)}^{\text{LW}}$ are the Richtmyer, or two-step Lax–Wendroff fluxes.

Going after the above procedure without several considerations, the numerical scheme may experience difficulties in solving discontinuous flows, and high frequency oscillations can appear in the numerical solution. A usual remission under such conditions is the use of an artificial viscosity term or shock fitting techniques to suppress steep gradients. These terms are case-based and require ad-hoc terms, thereafter should be adjusted by a careful calibration or a trial and error procedure.

Shock-capturing numerical method is a robust way that reproduces proper results for a problem with discontinuities within the computational domain. MUSCL is a well-known methodology for spatial discretization of NLSW equations. Based on MUSCL method, a non-linear limiter is employed to produce a piecewise linear reconstruction within each computational cell. The data reconstruction technique provides the conservative variables at cell interfaces as a linear extrapolation from the stored cell center data which are known either by the solution of previous time step or by the initial condition. Using a usual piecewise linear reconstruction for the second component of the vector of conservative variables, i.e., unit width discharge hu , yields:

$$(hu)_{i+(1/2),j}^- = (hu)_{i,j} + \frac{1}{2}(\Delta x)\delta_{i,j}(hu)$$

$$(hu)_{i+(1/2),j}^+ = (hu)_{i+1,j} - \frac{1}{2}(\Delta x)\delta_{i+1,j}(hu) \quad (19)$$

Hereafter, the superscripts “-” and “+” indicate evaluation on, respectively, the left and right hand sides of the interface indicated by the associated subscript. The limited slopes in (19) can be written as:

$$\delta_{(i,j)}(hu) = \Psi_{(i,j)} \quad (20)$$

In this equation, $\Psi_{i,j}$ is the slope limiter. Toro listed different slope limiters which can be used to provide a suitable choice of gradient in each computational cell, thus, giving an oscillation-free solution in the vicinity of shocks [9]. The Minmod limiter is an example:

$$\Psi(a,b) = \max(0, \min(a,b)) \quad (21)$$

where:

$$a = \frac{(hu)_{i+1,j} - (hu)_{i,j}}{\Delta x}, \quad b = \frac{(hu)_{i,j} - (hu)_{i-1,j}}{\Delta x} \quad (22)$$

The above procedure can be used for other components of the vector of conservative variables.

Up to this step, a numerical scheme is presented that is capable of solving the hydrodynamic governing equations in the presence of flow discontinuity. However, this efficient performance is held only for horizontal, frictionless bottoms. To overcome this problem, there are several different methods for incorporating source term into finite volume schemes. One of them is SGM. SGM appears to be a simple technique for the treatment of source term in NLSW equations. This approach was developed by [11] and found to be no more complicated than traditional methods for the homogeneous terms.

In this technique, the free surface elevation η , is chosen as the basis of data reconstruction, and the source term is discretized with a centered scheme. First, the reconstructed values of free surface elevation are obtained by the same method as used for unit width discharge, and then the corresponding values of water depth are calculated as:

$$\begin{aligned} h_{i+(1/2),j}^- &= \eta_{i+(1/2),j}^- - z_{b(i+(1/2),j)}, \\ h_{i,j+(1/2)}^- &= \eta_{i,j+(1/2)}^- - z_{b(i,j+(1/2))} \end{aligned} \quad (23)$$

where $z_{b(i+(1/2),j)}$ and $z_{b(i,j+(1/2))}$ are the bed elevations at the cell interfaces $i + (1/2), j$ and $i, j + (1/2)$, respectively. This reconstruction scheme fully retains the conservative property of the governing equations and reduces interpolation errors considerably.

It has been demonstrated that FORCE- MUSCL scheme satisfies the C-property when combined with SGM [12]. It means that starting from the stationary state conditions at an arbitrary time level, flow variables remains constant for all time levels. This property allows simulation of flows over irregular beds and becomes important when modeling small deviations from the steady state condition.

Subsequent to proper spatial discretization, (17) should be integrated along time axis. Optimal fourth-order Runge-Kutta method can be employed which is a popular time-stepping scheme for hyperbolic conservation laws.

Equation (17) shows a dynamic system which can be simulated by the following ordinary differential equation:

$$\frac{d\mathbf{U}}{dt} = \mathbf{P}(\mathbf{U}) \quad (24)$$

The fourth order Runge-Kutta algorithm (RK-4) integrates (17) [13].

Since RK-4 is an explicit time integrating algorithm then Courant-Friedrichs-Lewy (CFL) criterion, which is defined as follows, should handle the time steps size:

$$\Delta t = C_n \left[\max \left(\frac{|U_{(i,j)}| + \sqrt{gh_{(i,j)}}}{\Delta x}, \frac{|V_{(i,j)}| + \sqrt{gh_{(i,j)}}}{\Delta y} \right) \right]^{-1}, \quad 0 < C_n \leq 1 \quad (25)$$

in which C_n is the Courant number.

Proposing a numerical solution for flow equations, now the Exner equation should be solved properly. As implied, fully coupled, semi-coupled and uncoupled forms are three kinds of approaches in numerical implementation of morphodynamic equations. Efficiency of fully coupled form in which NLSW and Exner equations are solved simultaneously, is confirmed in previous researches. Therefore, in this research, the explained numerical scheme is generalized for solving the system of (12). In this end, the main question is how to approximate bed load sediment discharge. Several empirical equations are proposed, however, they are defined for specific experimental situations. In this research, a trained MLP ANN which is of FFBP type is applied for estimating sediment discharge. The ANN consists of an input and output layers which are related through a hidden layer with 22 neurons. For training the ANN, 1002 data are used. Furthermore, 500 data are employed for testing. These data are gathered from 842 flume experiments and 660 field data [14]. The input data include flow discharge, channel width, flow depth, water surface slope, sediment particle size mean diameter and specific gravity of sediment particles and the output is bed load. Some of the statistics features of input and output data are listed in Table I.

TABLE I
STATISTICS FEATURES OF INPUT AND OUTPUT DATA OF ANN

Data	Max.	Min	Ave.
Flow Discharge (m ³ /s)	575	0.001	73.6
Channel Width (m)	245.5	0.149	41.2
Flow Depth (m)	4.3	0.01	0.93
Water Surface Slope	0.0234	0.000037	0.0024
Sediment Particle Size Mean Diameter (mm)	28.5	0.01	2.38
Specific Gravity of Sediment Particles	4.22	1.25	2.64
Bed load (kg/m ³)	9.8	2e-6	1.08

IV. RESULTS AND DISCUSSIONS

Following the numerical model construction, it should be verified through several proper problems. This verification for hydrodynamic part involves dam-break on a dry bed channel with varying width. Then, the fully coupled morphodynamic model is employed for simulation of bed variations in an

alluvial junction and bed form modeling.

A. Hydrodynamic Module Verification

Dam-break flow onto a locally non-prismatic converging-diverging channel with initially dry bed conditions is modeled for showing the capability of the model to simulate flow discontinuities, transcritical flows, wetting/drying conditions and non-prismatic channel flows.

Several investigators have employed this test to verify their scheme capabilities in modeling real fluid flows [15]-[17].

Due to non-prismatic shape of the channel a proper way for modeling the boundary should be presented. Mapping techniques and unstructured meshes are usual methods that may be proposed for this purpose. However, it should be denoted that in spite of vitalities of mapping techniques, the governing equations may need to be transformed from the physical domain to the other imaginary computational domain, which sometimes needs a huge amount of mathematical calculations. Furthermore, if the entire computational domain is spatially discretized by applying unstructured meshes, then SGM may lead to undesirable results [18]. Accordingly, in this research, CCCM is suggested as an efficient technique for considering non-prismatic boundary conditions.

The CCCM has been developed by Centre of Mathematical Modeling and Flow Analysis Manchester Metropolitan University, to define grids in computational domains to solve the NLSW equations [19]. In CCCM, background Cartesian meshes are cut by several boundary curves, thus there is no conventional mesh generation which is required. In this method, the intersection points of boundary curves and background Cartesian meshes should be determined in the first step. Details have been explained in [19] and [20]. Toward this process, three kinds of cells may be reproduced: flow cells, cut cells and solid cells. The solid cells are indeed out of the computational domains. Also, the flow cells are treated in a straightforward manner that explained before. However, the cut cells are required to be taken into account for several remarks in reconstruction and numerical flux calculation processes.

According to Fig. 1 and (16), m (number of cell sides) may be changed from 3 to 5. It means that a cut cell may have an irregular shape other than single rectangular shape. Then, FORCE-MUSCL scheme should be adapted for the new computational cell shapes.

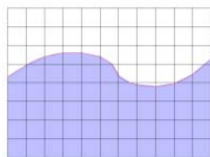


Fig. 1 Different kinds of meshes reproduced toward using CCCM [19]

It should be mentioned that the numerical flux, E^* , in (16) should be recalculated for the new shaped cut cells. As proposed by [9], the numerical FORCE flux for an irregular unstructured cell is:

$$\begin{aligned} \mathbf{F}^{LF}(\mathbf{U}^+, \mathbf{U}^-) &= \frac{|S^+| \mathbf{F}(\mathbf{U}^-) + |S^-| \mathbf{F}(\mathbf{U}^+)}{|S^-| + |S^+|} - \frac{2}{\Delta t} \frac{|S^+| |S^-|}{|S^-| + |S^+|} (\mathbf{U}^+ - \mathbf{U}^-) \\ \mathbf{F}^{LW} &= \mathbf{F}(\mathbf{U}^{LW}) \\ \mathbf{U}^{LW} &= \frac{|S^-| (\mathbf{U}^-) + |S^+| (\mathbf{U}^+)}{|S^-| + |S^+|} - \frac{\Delta t |S^0|}{2(|S^-| + |S^+|)} (\mathbf{F}(\mathbf{U}^+) - \mathbf{F}(\mathbf{U}^-)) \\ \mathbf{F}^{FORCE} &= \frac{1}{2} (\mathbf{F}^{LF} + \mathbf{F}^{LW}) \end{aligned} \tag{26}$$

\mathbf{U}^+ and \mathbf{U}^- are the values of reconstructed flow variables in the left and right side of a cell edge. Furthermore, S^+ and S^- are the surrounding area about the cell edge, and S^0 is the edge length.

Now, the efficient numerical model is produced for solving the problem. Fig. 2 shows the channel configuration in which there is a gate 6.1 m from upstream of the channel and 0.5 m wide. The channel constriction begins 7.9 m downstream of the gate, and then, the channel width reduces to 0.1 m by transition walls which makes 45° angle with the main channel walls. The constriction is 1 m long and 0.1 m wide. After the constriction, channel returns to its original width with diverging transition walls.

The initial channel depth before the gate is 0.3 m and constant Manning coefficient equal to 0.01 is used for all parts of the channel. Reflective boundary condition is set for the upstream, and transmissive boundary condition is used for the downstream. The depth history for 10 seconds after dam-break has been measured using four gages in laboratory [19]. The gages are installed at the channel centerline (Fig. 2).

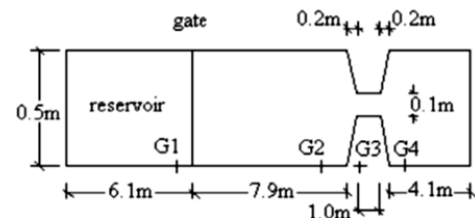


Fig. 2 Experimental layout of dam-break on a dry bed channel with varying width test

For imposing dry bed as the initial condition for the channel bed, few considerations should be taken into account. Following [21], a local minimum water depth h_{min} is defined in the scheme. To have a well posed problem, this threshold depth should be initially assigned to all physically dry cells, i.e. the cells located above the undisturbed water surface. During the computation, if the water depth h in a computational cell is below the threshold depth, then it will be set to h_{min} , the momentum (hu and hv) will be set to zero, and the cell is considered “dry”, otherwise the cell is considered “wet”. Moreover, the above procedure should be implemented in the reconstruction process. In this problem, $h_{min}=0.003$ was adopted.

Fig. 3 shows simulation results and the corresponding

laboratory measurements. Less than 1 s after the dam-break, the water wave reaches to gage 1 (Fig. 3 (a)). Rarefaction wave propagates downstream of the gate and the water depth drops rapidly for about 4 seconds. After that, the water depth drops with relatively slow rate. The shock front of the wave arrives at gage 2 after about 3 s and links to relatively low positive slope line which shows slow increasing in water depth (Fig. 3 (b)). Reaching reflected shock waves from the

constriction to gage 2, at $t=8$ s, the other wave front appears (Fig. 3 (b)). The model results for gage 3 show only one shock front (Fig. 3 (c)) because the constriction reflected waves propagate upstream-wise. Fig. 3 (d) shows the water depth history for gage 4 which is located after the constriction. In all of the figures, the computed results obtained in this research are compared with those held by [17] that are calculated through using the 2D numerical scheme presented by [22].

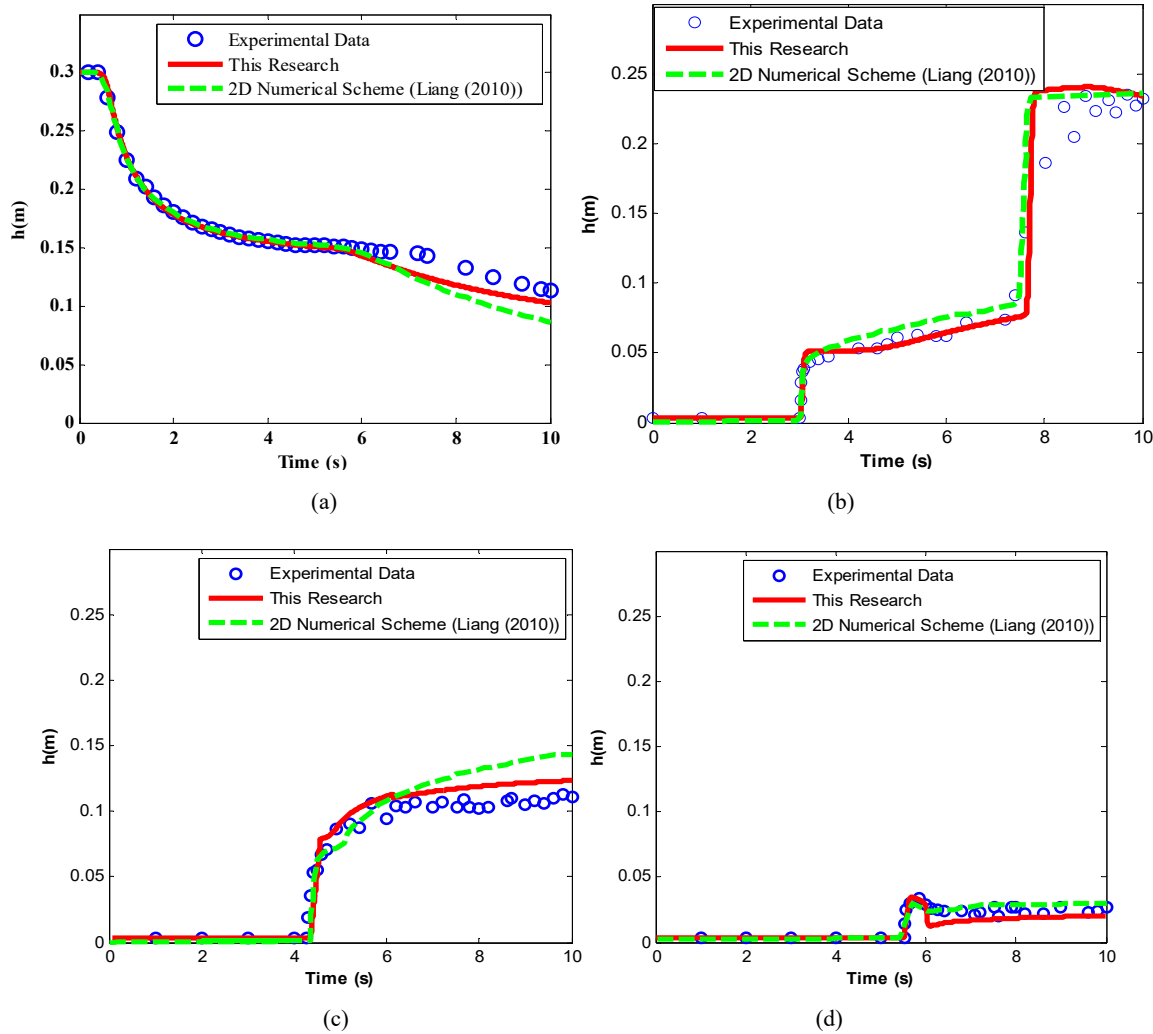


Fig. 3 Numerical results and experimental measurements for dam-break on a dry bed channel with varying width

As it can be seen in Figs. 3 (a)-(d), the model can track the trend of laboratory results very well. There are only few inconsistencies between the model results and measured data in gages 1 and 3 which also exist in some other reported finite volume models [15], [16]. These disagreements are attributable to different causes such as hydrostatic pressure assumption in shallow water equations that is insufficient for this problem with highly 3D features.

B. Dam-Break on a Dry Movable Bed

The interaction of mobile initially flat bed and a surge developed by a dam break is investigated in this example. The experimental setup was designed by [23]. The laboratory tests

were carried out in a 2.5-m length flume. The initial water depth before the simulated dam was 10 cm, and the flume bed was covered with PVC pellets with relative density of 1.54 and mean size diameter of 3.5 mm. The dam was opened suddenly.

Fig. 4 shows the time history of the bed evolution at a point which is located 25 cm before the dam. Dividing time by $t_0 = \sqrt{H_0/g}$, and bed elevation by initial water depth before the dam H_0 , the nondimensionalized time and bed height axes are defined. In this figure, the results of the numerical scheme in cooperating with ANN and those obtained through applying four well-known empirical formulas, in order to estimate

sediment discharge, are compared with the experimental measurements. In spite of existence of a flow shock and wetting/drying conditions, a reasonable tracking of the experimental measurements can be seen. All of the curves in the figure can capture the initial flushing and subsequently aggradation. However, a relatively better performance of ANN rather than the empirical formulas is evident. Furthermore, Fig. 5 depicts the time history of changes in the water surface. More accurate results of ANN can be deduced from this figure too.

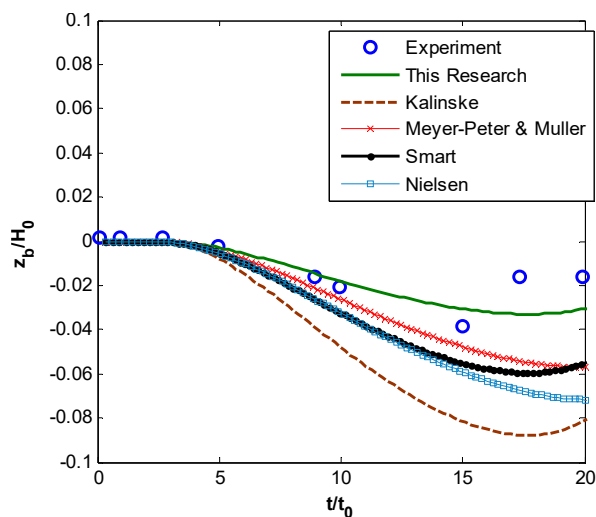


Fig. 4 Time history of the bed evolution

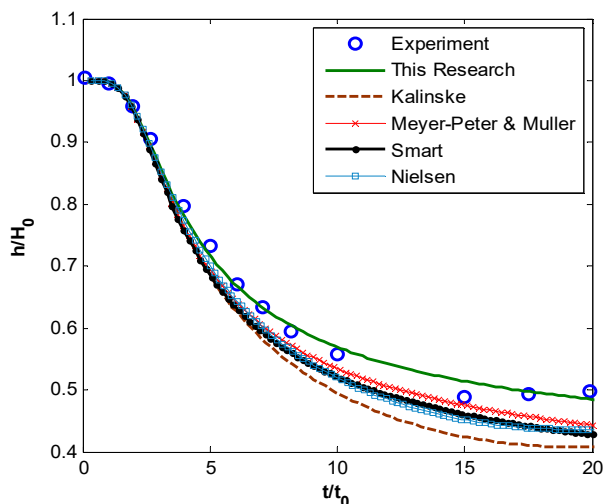


Fig. 5 Time history of changes in the water surface

C. Bed Variations in an Alluvial Junction

A main channel and some tributaries are a usual configuration in a natural channel. Hydrodynamics of intersection of the main channel and tributaries which is called a junction is very complicated, especially when movable bed situations are considered. A scheme capability in modeling bi-directional flows can be verified by simulating the flow at a channel junction. Ghobadian and Shafai Bajestan set up several experiments on 90° open channel junctions [24]. The

main and the tributary flumes took several width and discharge ratios in their experiments. Among these tests, a case in which the flow rate and channel width were $Q=0.16 \text{ m}^3/\text{s}$ and $w=0.35 \text{ m}$ for the main channel and $Q=0.04 \text{ m}^3/\text{s}$ and $w=0.25 \text{ m}$ for the tributary channels, respectively, was selected for verifying the numerical model. The initial flow depth in both channels is 12.75 cm, the sandy movable bed thickness is 11 cm, and the bed material mean diameter size is 1.05 mm.

Fig. 6 shows the results of the numerical scheme for bed evolutions by applying the trained ANN for estimating sediment discharge. The simulated patterns are tracking those which were described by [24]. In order to reach a quantitative comparison, the results of the numerical scheme using ANN for estimating maximum height of aggradation and minimum depth of degradation is compared with those collaborating specified empirical formulas. It can be seen that employing ANN leads to more accurate results in comparison with those which are achieved through using the empirical formulas. Overall, a proper agreement between the results of the numerical model and experimental measurements in an alluvial junction can be deduced.

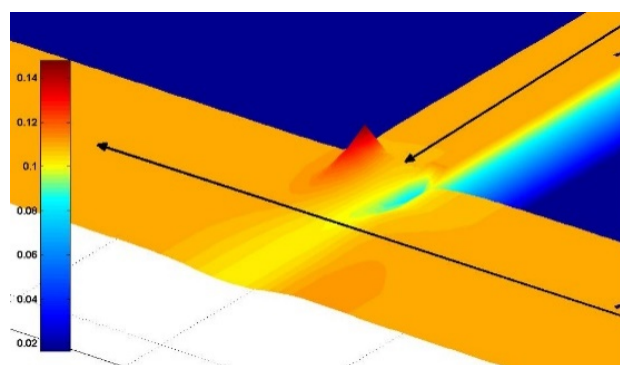


Fig. 6 The numerical model results for bed elevation changes in the alluvial channel junction

V. CONCLUSIONS

In this research, a numerical morphodynamic model is introduced which solves NLSW and Exner equations in fully coupled form. A combination of FORCE and MUSCL is held to achieve a high order accuracy scheme for spatial discretization of the computational domain, and SGM is used as a simple technique to treat the source term and satisfy C-property without using any ad-hock terms. Combining fourth order Runge-Kutta for time integration and CCCM for holding mesh generation in non-prismatic channel problems with the mentioned scheme produces an expert numerical model. Furthermore, a trained MLP ANN which is of FFBP type estimates sediment flow discharge in the model rather than usual empirical formulas.

Dam-break on a dry bed channel with varying width is an example that demonstrates the capability of the hydrodynamic part of the model in capturing the flow discontinuities, simulating transcritical flows and solving wetting/drying problems even in non-prismatic channels. Moreover, dam

break on a dry movable bed and bed level variations in an alluvial junction are used as several verifying problems for the fully coupled morphodynamic part of the model. The results show that the model is capable of presenting proper results for movable bed situations. It can also be deduced that applying ANN, instead of common empirical formulas for estimating flow discharge, leads to more accurate results.

REFERENCES

- [1] E.F. Toro, A. Siviglia, "PRICE: primitive centred schemes for hyperbolic system of equations," *International Journal for Numerical Methods in Fluids*, 2003, 42, pp.1263–1291.
- [2] W. Wu, "Depth-averaged two-dimensional numerical modeling of unsteady flow and nonuniform sediment transport in open channels," *Journal of Hydraulic Engineering*, 2004, 130 (10), pp. 1013–1024.
- [3] S. S. Li, R. G. Millar, "Simulating bed-load transport in a complex gravel- bed river," *Journal of Hydraulic Engineering*, 2007, 133(3), pp.323–328.
- [4] A. Canestrelli, A. Siviglia, M. Dumbser, E. F. Toro, "Well-balanced high-order centered schemes for non-conservative hyperbolic systems, Applications to shallow water equations with fixed and mobile bed," *Advances in Water Resources*, 2009, 32, pp. 834–844.
- [5] J. Murillo, P. Garcia-Navarro, "An Exner-based coupled model for two-dimensional transient flow over erodible bed," *Journal of Computational Physics*, 2010, 229, pp. 8704–8732.
- [6] M. Postacchini, M. Brocchini, A. Mancinelli, M. Landon, "A multi-purpose, intra-wave, shallow water hydro-morphodynamic solver," *Advances in Water Resources*, 2012, 38, pp. 13–26.
- [7] S. Cordier, M. H. Le, T. Morales de Luna, "Bedload transport in shallow water models: Why splitting (may) fail, how hyperbolicity (can) help," *Advances in Water Resources*, 2011, 34, pp. 980–989.
- [8] J. Smagorinsky, "General circulation experiments with the primitive equations, I. The basic experiments," *Monthly Weather Review*, 1963, 91(2), pp. 99–164.
- [9] E. F. Toro, *Shock-capturing methods for free-surface shallow flows*. Wiley: West Sussex, England, 2001.
- [10] E. F. Toro, *Riemann solvers and numerical methods for fluid dynamics*. Third Edition, Springer: Germany 2009.
- [11] J. G. Zhou, D. M. Causon, C. G. Mingham, D. M. Ingram, "The surface gradient method for the treatment of source terms in the shallow water equations," *Journal of Computational Physics*, 2001, 168(1), pp. 1–25.
- [12] S. M. Amiri, N. Talebbeydokhti, A. Baghlani, "A two-dimensional well-balanced numerical model for shallow water equations," *Scientia Iranica*, 2013, 20 (1), pp. 97–107.
- [13] I. K. Nikolos, A. I. Delis, "An unstructured node-centered finite volume scheme for shallow water flows with wet/dry fronts over complex topography," *Computer Methods in Applied Mechanics and Engineering*, 2009, 198, pp. 3723–3750.
- [14] W. R. Brownlie. *Compilation of alluvial channel data: laboratory and field*. W. M. Keck Laboratory of Hydraulics and Water Resources Division of Engineering and Applied Science California Institute of Technology Pasadena, California 1981; Report No. KH-R-43B.
- [15] P. Brufau, P. Garcia-Navarro, "Two-dimensional dam break flow simulation," *International Journal of Numerical Methods in Fluids* 2000, 33, pp. 35–57.
- [16] N. Goutal, F. Maurel, "A finite volume solver for 1D shallow-water equations applied to an actual river," *International Journal of Numerical Methods in Fluids*, 2002, 38, pp. 1–19.
- [17] N. A. Alias, Q. Liang, G. Kesserwani, "A Godunov-type scheme for modeling 1D channel flow with varying width and topography," *Computers and Fluids*, 2011, 46, pp. 88–93.
- [18] A. Mohamadian, D. Y. Le Roux, M. Tajrishi, K. Mazaheri, "A mass conservative scheme for simulating shallow flows over variable topographies using unstructured grid," *Advances in Water Resources*, 2005, 28, pp. 523–539.
- [19] J. A. Alvarez, *Towards the numerical simulation of ship generated waves using a cartesian cut cell based free surface solver*, Ph. D. Thesis: Centre of Mathematical Modeling and Flow Analysis Department of Computing and Mathematics Manchester Metropolitan University 2008.
- [20] D. M. Causon, D. M. Ingram, C. G. Mingham, G. Yang, R. V. Pearson "Calculation of shallow water flows using a cartesian cut cell approach," *Advances in Water Resources*, 2000, 23, pp. 545–562.
- [21] A. Mahdavi, N. Talebbeydokhti, "Modeling of non-breaking and breaking solitary wave run-up using FORCE-MUSCL scheme," *Journal of Hydraulic Research*, 2009, 47 (4), pp. 476–485.
- [22] Q. Liang, "Flood simulation using a well-balanced shallow flow model," *ASCE Journal of Hydraulic Engineering*, 2010, 136(9), pp. 669–675.
- [23] B. Spinewine, Y. Zech, "Dam-break waves over movable beds: a flat bed test case," 2nd IMPACT workshop, Statkraft Grøner, Mo-i-Rana 2002.
- [24] R. Ghobadian, M. Shafai Bajestan, "Investigation of sediment patterns at river confluence," *Journal of Applied Science* 2007, 7(10), pp. 1372-1380.